Polychromatic solar energy conversion in pigment-protein chimeras that unite the two kingdoms of (bacterio)chlorophyll-based photosynthesis

Juntai Liu,[1] Vincent M. Friebe,[2] Raoul N. Frese[2] and Michael R. Jones[1*]

[1]School of Biochemistry, Faculty of Life Sciences, Biomedical Sciences Building, University of Bristol, University Walk, Bristol BS8 1TD, United Kingdom.

[2]Department of Physics and Astronomy, LaserLaB Amsterdam, VU University Amsterdam, De Boelelaan 1081, Amsterdam 1081 HV, The Netherlands.

*Corresponding author (m.r.jones@bristol.ac.uk)

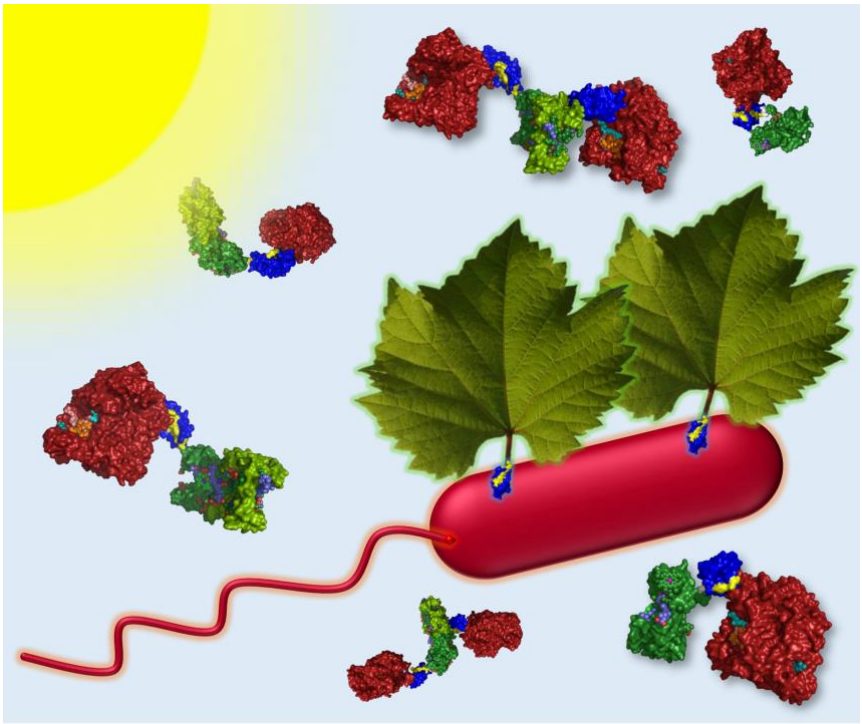

ToC image

Natural photosynthesis can be divided between the chlorophyll-containing plants, algae and cyanobacteria that make up the oxygenic phototrophs and a diversity of bacteriochlorophyll-containing bacteria that make up the anoxygenic phototrophs. Photosynthetic light harvesting and reaction centre proteins from both groups of organisms have been exploited in a wide range of biohybrid devices for solar energy conversion, solar fuel synthesis and a variety of sensing technologies, but the energy harvesting abilities of these devices are limited by each protein's individual palette of (bacterio)chlorophyll, carotenoid and bilin pigments. In this work we demonstrate a range of genetically-encoded, self-assembling photosystems in which recombinant plant light harvesting complexes are covalently locked with reaction centres from a purple photosynthetic bacterium, producing macromolecular chimeras that display mechanisms of polychromatic solar energy harvesting and conversion not present in natural systems. Our findings illustrate the power of a synthetic biology approach in which bottom-up construction of a novel photosystem using naturally disparate but mechanistically complementary components is achieved in a predictable fashion through the genetic encoding of adaptable, plug-and-play covalent interfaces.

Our everyday experience of photosynthesis is dominated by the blue/red-absorbing pigment chlorophyll, a magnesium tetrapyrrole that acts as both a harvester of solar energy and a carrier of electrons and holes. Variants of this versatile molecule, principally chlorophyll *a* and chlorophyll *b*, are found in the plants, algae and cyanobacteria that make up the oxygenic phototrophs. Less obvious are the anoxygenic phototrophs, bacteria that use electron donors other than water and have one or more variants of bacteriochlorophyll as their principal photosynthetic pigment. Although these bacteria are less obvious in our environment, oxygen-tolerant species are widespread in oceanic surface waters where they make a sizeable contribution to global solar energy conversion[1]. A few species, including the bacteriochlorophyll *a*-containing *Rhodobacter* (*Rba.*) *sphaeroides*, have played major roles in our understanding of excitation energy transfer in light harvesting "antenna" complexes (LHCs)[2–4] and charge separation in photochemical reaction centres (RCs)[5,6].

Improving the performance of photosynthesis and finding new ways to exploit natural solar energy conversion have become important research topics[7,8], and there is growing interest in the use of photosynthetic proteins as environmentally-benign components in biohybrid devices for solar energy conversion[9–14]. Photoexcitation of a RC in such a device triggers intra-protein charge

separation, producing a potential difference between opposite "poles" of the protein that drives subsequent electron transfer to create a photocurrent and photovoltage. In addition to solar energy conversion *per se*, proposed applications of photoprotein devices have included biosensing, light/UV sensing, touch sensing and solar fuel synthesis[9–16]. Photosynthetic proteins are attractive as device components because they are environmentally sustainable and benign, they achieve solar energy conversion with a very high quantum efficiency (charges separated per photon absorbed), and they can be adapted to purpose through protein engineering. However, a limitation is their selective use of available solar energy[7,8], a consequence of their particular palette of light harvesting pigments (Fig. 1a). This can be evidenced in devices through the recording of action spectra of external quantum efficiency (EQE – the number of charges transferred per incident photon), which exhibit peaks and troughs that correspond to the absorbance spectra of the particular light harvesting pigments that are coupled to charge separation in the device[12,17–21].

A striking observation is the complementary nature of the absorbance spectra of chlorophyll and bacteriochlorophyll photosystems (Fig. 1a). This is enabled by the somewhat different electronic structures of their principal pigments (Supplementary Fig. S1a) and facilitates the occupancy of complementary ecological niches by oxygenic and anoxygenic phototrophs. Chlorophyll absorbs most strongly in the blue and red whereas the absorbance of bacteriochlorophyll is shifted to the near-ultraviolet and near-infrared. The absorbance spectra of plant and bacterial carotenoids between 400 and 600 nm are also somewhat complementary (Fig. 1a). Thus, anoxygenic phototrophs harvest parts of the solar spectrum which oxygenic phototrophs do not absorb well, and *vice versa*.

Following nature's lead, here we present the use of genetic encoding to achieve the self-assembly, from disparate components, of novel photoprotein "chimeras" that display polychromatic solar energy harvesting and conversion (Fig. 1b,c). The components are the *Rba. sphaeroides* RC[5,6] and the LHCII[22–25] and LHCI[26–30] proteins from *Arabidopsis thaliana* (Supplementary Fig. S1b-e). Highly specific and programmable self-assembly is achieved through adaptation of these components with the constituents of a two-component protein interface domain that covalently locks together photosynthetic membrane proteins with no natural propensity to associate. The resulting macromolecular, adaptable chimeric photosystems have defined compositions, and display novel mechanisms of solar energy conversion across the near-UV, visible and near-IR.

Results

Solar energy conversion by unadapted photosystem components

We first looked at whether unadapted plant LHCIIs can pass harvested energy to unadapted purple bacterial RCs in dilute solution. On receipt of excitation energy, photochemical charge separation in the *Rba. sphaeroides* RC is a rapid four-step process (Fig. 1d) that produces a metastable oxidised primary electron donor ($P870^+$) and reduced acceptor ubiquinone (Q_B); energy transfer can therefore be detected as a quenching of LHC emission accompanied by an enhancement of P870 oxidation. Although unadapted bacterial RCs and plant LHCIIs (see Methods for sources) have overlapping absorbance and emission spectra between 600 nm and 800 nm (Fig. 1b) no appreciable energy transfer was observed when they were mixed in solution because they have no capacity for binding to one another. The addition of purified wild-type (WT) RCs did not significantly reduce emission from LHCII (Fig. 2a) and photo-oxidative bleaching of this RC's P870 primary electron donor absorbance band in response to 650 nm excitation was not significantly enhanced by the addition of LHCII (Fig. 2b) which absorbs strongly at this wavelength (Fig. 1b).

In comparison to LHCII, the spectral overlap (*J*) between LHC emission and RC absorbance is ~80 % larger in the case of LHCI (Fig. 1c and Table 1) which contains a pair of "red-form" chlorophyll *a* that possess a charge-transfer state that mixes with the low energy exciton state[30]. Although the addition of WT RCs did bring about a decrease in LHCI emission (Fig. 2a) there was no associated significant increase in RC P870 photobleaching in the presence of LHCI (Fig. 2c), leading to the conclusion that the observed emission quenching was not due to energy transfer. Protein concentrations used for the fluorescence measurements were too low (max absorbance < 0.07) for this LHCI quenching to be attributable to reabsorption by RCs, and equivalent quenching was not seen with LHCII at a similar concentration (Fig. 2a). As it is known that the emission quantum yield of LHCI is much more sensitive to its *in vitro* environment than is the case for LHCII[28], the observed drop in LHCI emission on adding RCs is attributed to a change in its intrinsic quantum yield.

To establish the principle that plant LHCs can pass energy to bacterial RCs when brought sufficiently close together, mixtures of unadapted LHC and RC proteins were adhered to a nanostructured silver cathode and their capacity for generating photocurrents examined (see Material and Methods). In this photoelectrochemical system (Fig. 2d) cytochrome *c* is used to "wire" charge separation in the RC to the cathode, and ubiquinone-0 (Q_0) shuttles electrons to the counter electrode[20,31,32]. Electrodes drop-cast with purified WT RCs produced a photocurrent in response to

RC-specific 870 nm light and a weaker current in response to 680 nm excitation where RC absorbance is very low (Supplementary Fig. S2a). An external quantum efficiency (EQE) action spectrum showed good correspondence with the RC absorbance spectrum, confirming that the photocurrent was attributable to light capture by the pigments of the RC (Fig. 2e, black versus red). As expected, an electrode fabricated with purified LHCII (or LHCI) failed to show any photocurrent response during excitation of the main LHCII absorbance band at 680 nm (Supplementary Fig. S2a) or at any other wavelength.

For electrodes fabricated from a mixture of unadapted WT RCs and LHCs, in addition to the expected RC bands the EQE spectra contained a component between 620 and 700 nm that corresponded to the low energy absorbance band of LHCII or LHCI (Fig. 2e, green). A contribution from the high energy Soret absorbance band of LHCII or LHCI was also evident (Supplementary Fig. S3b,c) when EQE spectra were recorded using a blue-enhanced light source (Supplementary Fig. S3a). This demonstrated (for the first time as far as we are aware) that photoexcited LHCII or LHCI chlorophylls can pass energy to the bacteriochlorophylls of a purple bacterial RC, producing charge separation and a photocurrent response. In this case this proximity-dependent effect was realised by bringing the two types of protein sufficiently close to one another on the surface of a biophotoelectrode.

Design and production of component for chimeric photosystems

In an attempt to activate chlorophyll to bacteriochlorophyll energy transfer in dilute solution, RCs and LHCs were adapted using the SpyTag/SpyCatcher protein fusion system[33] as a programmable interface. When mixed in solution, highly-specific binding of the short SpyTag peptide to the SpyCatcher protein domain initiates autocatalysis of an isopeptide bond between the two involving aspartate and lysine residues (Supplementary Fig. S1f), producing a single, covalently-locked, water-soluble protein domain. Using synthetic genes, the SpyCatcher protein was fused to the RC and the short SpyTag peptide to recombinant LHCII or LHCI, creating adapted components that could be expressed independently using *Rba. sphaeroides* or *E. coli*, respectively (see Materials and Methods).

To adapt the RC an optimized version of SpyCatcher[34], 106 amino acids in length (SpyCatcherΔ), was attached to the N-terminus of the RC PufL protein either directly (RC*C*) or via a four (RC*4C*) or eight (RC*8C*) amino acid linker (Fig. 3a and Supplementary Table S1). Adapted RC proteins were expressed in *Rba. sphaeroides*. For LHCII, Lhcb apoproteins were expressed in *E. coli*

and mature pigment-protein monomers refolded *in vitro* with purified pigments[35–38]. Four LHCII proteins were designed (Fig. 3b, and see Supplementary Fig. S4a for protein sequences). The first lacked twelve dispensable N-terminal amino acids that are not resolved in available X-ray crystal structures[22–24] and had a His-tag at its C-terminus. This "dLHCII" protein was used as the control LHCII complex for all measurements. The remaining three had either the full 13 amino acid SpyTag peptide or a truncated 10 amino acid SpyTagΔ variant added to the N-terminus of the truncated Lhcb1 (T-dLHCII and Td-dLHCII, respectively) or SpyTag added to the C-terminus of the full Lhcb1 (LHCII-T) (Fig. 1b).

Adapted heterodimeric LHCI proteins (Fig. 3c) were also refolded from apoproteins expressed in *E. coli*[26,30,39,40]. This involved mixing SpyTagΔ-adapted Lhca4 protein (Td-L4) with either unadapted Lhca1 protein (L1) or SpyTagΔ-adapted Lhca1 protein (Td-L1), to produce LHCI either singly or doubly modified with SpyTagΔ (termed LHCI-Td and Td-LHCI-Td, respectively). This enabled the creation chimeras between LHCI and either one or two RCs.

Self-assembly of RC-LHC chimeras

When incubated together, all possible pairwise combinations of adapted RCs and LHCIIs efficiently formed a stable higher molecular weight product, dubbed a chimera, that could be visualised on sucrose density gradients. Unadapted RCs and LHCIIs could be distinguished on sucrose density gradients as discrete red and green bands (Fig. 3d, gradients 1,2), as could components in mixtures incapable of forming chimeras (Fig. 3d, gradients 3,4). However, mixing any SpyCatcherΔ-adapted RC with any SpyTag-adapted LHCII produced a product that migrated further than either monomeric protein. The two examples shown (Fig. 3d, gradients 5,6) are LHCII#RC chimeras from a RC*C*/LHCII-T mix and RC*4*#dLHCII chimeras from a RC*4C*/Td-dLHCII mix (where "#" denotes the spontaneously-formed SpyCatcher/SpyTag interface domain). Chimera formation could also be detected on a native blue gel (Supplementary Fig. S5a), and SDS-PAGE combined with western blotting using anti-His antibodies confirmed that chimera self-assembly was due to the formation of a covalent fusion protein between the SpyTag- or SpyTagΔ-adapted Lhcb1 polypeptide of LHCII and the SpyCatcherΔ-adapted PufL polypeptide of the RC (Supplementary Fig. S5b).

A change in protein morphology on chimera formation was also evident from transmission electron microscopy (TEM). Images of a mix of unadapted WT RCs and dLHCII showed a large number of monodispersed, regularly-sized objects of <10 nm diameter (Fig. 3e, left), whereas images of the purified LHCII#RC chimera revealed larger, evenly-distributed elliptical structures of

>10 nm diameter along the longest axis (Fig. 3e, right). A molecular model of this chimera, based on available X-ray crystal structures for the RC, LHCII and SpyCatcher/Tag, is shown in Fig. 3f.

RC-LHCI and $(RC)_2$-LHCI chimeras were assembled by incubation of LHCI-Td or Td-LHCI-Td with a three-fold excess of RC*C*. This again produced higher molecular weight products that could be separated from unreacted RCs on blue native gels (Fig. 3g). As designed, assembly of RC*C* with doubly-adapted Td-LHCI-Td complexes produced higher molecular weight products than with singly-adapted LHCI-Td complexes (Fig. 3g, right). Equivalent results were obtained with LHCI adapted with the full SpyTag and also with RC*4C* (Supplementary Fig. S6a). Analysis by SDS-PAGE and western blotting confirmed that chimera self-assembly was due to spontaneous formation of fusion proteins between the SpyCatcherΔ-adapted PufL of the RC and the SpyTagΔ-adapted Lhca4 and Lhca1 (Supplementary Fig. S6b). Chimeras formed from RC*C* were selected for further analysis as these had no linker between the SpyCatcher/Tag domain and the RC. Molecular models of these chimeras, dubbed LHCI#RC and RC#LHCI#RC, are shown in Fig. 3h. Sucrose density gradient ultracentrifugation (Fig. 3i) showed that LHCI#RC chimeras (gradient 5) were clearly larger than LHCI alone (gradients 2-4) or unadapted RCs (gradients 1,3,4), and RC#LHCI#RC chimeras (gradient 6) were larger again. Covalent-locking of the structure enabled purification of all LHCI-RC and LHCII-RC chimeras with the designed molar ratio (Supplementary Fig. S5c and S6c).

Chlorophyll to bacteriochlorophyll energy transfer in chimeras

In solution, the nine chimeras formed between RCs and LHCIIs exhibited between 14 and 27 % less LHCII emission than a control sample formed from an equivalent mix of the SpyTag-adapted LHCII and WT RCs (Fig. 4a – and see spectra in Supplementary Fig. S7A). This was diagnostic of energy transfer, probably through a Förster resonance energy transfer (FRET) mechanism at the distances implied by the chimera models (Fig. 3f,h), that was activated by physically-linking the RC to the LHCII. For the chimeras based on LHCIIs with SpyTag at the N-terminus the extent of emission quenching did not seem to depend on the type of SpyCatcher-adapted RC, but for those based on the LHCII with SpyTag at the C-terminus the quenching seemed to be greater for RC*s* with a shorter linker to the SpyCatcher module (Fig. 4a, right). These trends, observed with 651 nm excitation, were also seen in data on the same complexes gathered with 475 nm excitation (Supplementary Fig. S7B). This lack of an excitation wavelength dependence showed that the LHCIIs in the chimeras were structurally intact and that the reduction in their LHCII emission was not due to parasitic RC absorbance (which would be expected to be wavelength dependent).

To confirm energy transfer from LHCII to the RC, measurements of RC P870 photo-oxidation in response to 650 nm excitation were carried out on LHCII#RC and RC*4*#dLHCII chimeras as examples where the LHCII was connected via either its N- or C-terminus. Bleaching of 870 nm absorbance was much stronger in LHCII#RC chimeras than in controls comprising the RC*C* alone, or a mixture of RC*C* with unadapted dLHCII complexes (Fig. 4c), and the same was found for the RC*4*#dLHCII chimera (Supplementary Fig. S8). Hence decreased emission by the LHCII energy donor was accompanied by enhanced photo-oxidation of the RC energy acceptor, confirming energy transfer between the two in solution.

Chimeras were also assembled using singly or doubly adapted LHCI. Greater quenching of LHCI emission was seen on forming LHCI#RC or RC#LHCI#RC chimeras with either RC*C* or RC*4C* than on mixing the same adapted LHCI with unadapted WT RCs (Fig. 4c). These findings were again independent of excitation wavelength (Fig. S9) showing they were not due to absorbance of excitation light by the tethered RC. This emission quenching was accompanied by significant enhancement of P870 photo-oxidation in LHCI chimeras with one or two RC*C*, compared to RC*C* alone (Fig. 4d), confirming energy transfer from LHCI to the RC in solution on formation of a chimera between the two.

Purified chimeras were adhered to nanostructured silver electrodes to test their functionality. Promisingly, all were able to generate photocurrents, showing that dynamic interactions between the RC, cytochrome *c* and ubiquinone at the electrode surface, required for the generation of a photocurrent, were not obstructed by attaching the RC to LHCII or LHCI. All EQE action spectra recorded for chimeras exhibited low energy (Fig. 4e,f) and high energy (Supplementary Fig. S3d,e) chlorophyll bands indicating photocurrent generation powered by LHC absorbance.

The probable mechanism of solar energy conversion operating in chimeras, based on what is known about the photophysics of these proteins, is summarised in Fig. 5. Energy captured by the pigment systems of LHCII or LHCI is passed to the RC, exciting the primary electron donor bacteriochlorophylls (P870*) and initiating charge separation to form $P870^{+}Q_{B}^{-}$. Energy harvested by the chlorophyll *b* (or carotenoid) pigments of either LHC is passed to the lower energy chlorophyll *a*. Inter-protein energy transfer is likely to involve a sub-set of red-shifted chlorophyll *a* in either LHC and entry into the RC is likely to occur principally via the bacteriopheophytin cofactors ($H_{A/B}$) as their absorbance has the greatest spectral overlap with LHC emission (Fig. 1c).

Energy transfer efficiency in chimeras

Apparent efficiencies of energy transfer from LHCII or LHCI to the RC were estimated in two ways (see Materials and Methods, Eqs. 2-5). The first (E_{FL}) was based on the additional quenching of LHC emission in a chimera relative to that in a compositionally-matched mixture of the relevant LHC variant and WT RCs (Eq. 2,3) or additional quenching in a LHC/WT RC mixture relative to that in a concentration-matched LHC-only sample. The second was from the accelerated rate of RC P870 photobleaching in a chimera relative to a matched RC-only control (E_{P870} – Eq. 4).

Values of E_{P870} calculated from experimental data are shown in Table 1. The efficiency of energy transfer was less than 4 % in mixtures of unadapted RCs with unadapted dLHCII, SpyTag-adapted LHCII or SpyTag-adapted LHCI, consistent with expectations for a dilute (500 nM) solution of two proteins that have no propensity to associate. In marked contrast E_{P870} was over 20 % in the corresponding RC-LHCII or RC-LHCI chimera. For all chimeras values of E_{FL} derived from LHC emission data were in agreement with values of E_{P870} derived from RC absorbance data (Table 1). This correspondence between independently-determined efficiencies from separate data sets reinforced the conclusion that energy transfer was taking place from the plant LHCs to the bacterial RCs within the chimera.

By either method the estimated efficiency of energy transfer in the RC#LHCI#RC chimera was higher than that in LHCI#RC chimera (Table 1), consistent with the presence of two acceptors in the former, but it was notable that it was not double. Estimates of the energy transfer efficiency to the second RC added to Lhca1, made using Eq. 5 in Materials and Methods, yielded values that were either 58 % or 69 % of that for transfer to the first RC attached to Lhca4. This is consistent with the presence in the Lhca4 subunit of the relatively low energy red-form chlorophyll *a* dimer (Supplementary Fig. S1d) that is responsible for the red-enhancement of the LHCI emission spectrum[28,30,39,40], and which may have produced more efficient energy transfer to an attached RC.

Also by either estimate, the efficiency of energy transfer in the LHCI#RC chimera was not significantly higher than either the LHCII#RC or RC*4*#dLHCII chimera despite a ~80 % stronger spectral overlap factor *J* (Table 1). This is likely due to the reconstituted LHCI heterodimers being in a partially quenched state, reducing the quantum yield to only 29 % of that of LHCII[28]. This was also the case in the present work where our quantum yield estimates were 30 % for LHCI-Td and 28 % for Td-LHCI-Td (Table 1). It is plausible that the ~70 % lower quantum yield of LHCI relative to LHCII offset the ~80 % stronger spectral overlap, producing similar energy transfer efficiencies in the LHCI and LHCII chimeras. In future work it might be possible to partially overcome this through

modification of LHCI in the native organism, as the quantum yield of native LHCI heterodimers has been reported to be ~64 % that of LHCII, more than double that of recombinant LHCI[28].

Conclusions

This work shows that genetically adapting two types of evolutionarily-disparate photosynthetic membrane proteins with an extramembrane interface domain enables self-assembly of a chimeric photosystem in which UV/near-IR solar energy conversion by a bacteriochlorophyll RC is augmented by visible light capture by chlorophyll LHCs. This approach inspired by a concept of synthetic biology, adapting naturally incompatible components to interface in a predictable way through genetic encoding, creates covalently-stabilised macromolecular photosystems that are predictable and programmable. In addition to providing novel photosynthetic structures and energy transfer pathways to explore, these polychromatic photosystems constitute interesting new materials for biohybrid devices that in recent years have expanded in application beyond photoelectrochemical solar energy conversion to fuel molecule synthesis, energy storage, biosensing, touch sensing and photodetection. Finally, the demonstrated flexibility with which RCs and LHCs could be interfaced opens the possibility of constructing more elaborate, self-assembling chimeric photosystems that employ multiple orthogonal linking modules[41,42] and a wider range of photosynthetic and redox proteins that, despite being separated by billions of years of evolution, can be adapted for future solar energy conversion through genetic programming of predictable interfaces.

Acknowledgements

The Lhcb1.3 plasmid was a kind gift from Prof. Roberta Croce from the Vrije Universiteit Amsterdam, The Netherlands. J.L and M.R.J acknowledge funding from the EPSRC/BBSRC Synthetic Biology Centre for Doctoral Training (EP/L016494/1) and from the BrisSynBio Synthetic Biology Research Centre at the University of Bristol (BB/L01386X/1). R.N.F acknowledges support from the Netherlands Organisation for Scientific Research (NWO) for a Vidi grant, and V.M.F for funding from NWO Veni project 16866.

Author contributions

J.L and M.R.J conceived the research. J.L. engineered the chimeras and characterised energy transfer. V.F and J.L carried out photochronoamperometry under supervision from R.F. J.L and M.R.J drafted the manuscript and all authors commented on the manuscript. M.R.J supervised the project.

Competing interests

The authors declare no competing interests.

Methods

RC modification and purification. SpyCatcherΔ, a version of the SpyCatcher protein lacking nine C-terminal amino acids that are not resolved in the X-ray crystal structure of SpyCatcher/SpyTag[34] was used in order to reduce the length of the linking peptide between the main bodies of the RC and SpyCatcher proteins. It was fused to the N-terminus of the RC PufL polypeptide, which is an alanine exposed at the protein surface on the cytoplasmic side of the membrane (white spheres in Supplementary Fig. S1a), either directly or via a four (SESG) or eight (SGESGESG) amino acid linker, and was preceded by a His-tag for purification (Fig. 3a). Nomenclature used for these and all other component proteins and chimeras are summarised in Supplementary Table S1. The required plasmids were constructed using synthetic DNA (Eurofins). The WT RC control was also modified with a His tag for purification as described previously[43]. All RCs were expressed in a strain of *Rba. sphaeroides* engineered to lack light harvesting complexes[43,44], were purified by nickel affinity chromatography and gel filtration[43], and were stored at -80 °C as a concentrated solution in 20 mM Tris (pH 8.0)/0.04 % DDM (Tris/DDM buffer).

LHCII modification, refolding and purification. To enable low-cost and rapid genetic modification of plant LHCII the designed apoproteins were expressed in *E. coli* and the mature pigment-proteins refolded in DDM using pigments purified from spinach[35]. Four modified LHCII were designed (Fig. 3b and Supplementary Fig. S4a). Complex dLHCII lacked twelve dispensable N-terminal amino acids that are not resolved in available X-ray crystal structures[22–24] (Supplementary Fig. S1d). This sequence, which includes four basic amino acids, is involved in stacking of thylakoid grana but can be removed without affecting core LHCII light-harvesting function[23]. Their removal minimised the

sequence linking the main body of LHCII (starting at serine 14) to additional components added at the N-terminus. In the second construct the 13 amino acid SpyTag peptide was added to the N-terminus of dLHCII to form T-dLHCII, whilst in the third construct a truncated SpyTagΔ was added to the N-terminus of dLHCII to form Td-dLHCII. This modified SpyTagΔ lacked three dispensable amino acids at its C-terminus[34], further reducing the linker to the N-terminus of LHCII. In the fourth construct the full 13 amino acid SpyTag peptide was added to the C-terminus of Lhcb1 after a three amino acid linker (termed LHCII-T). In all cases a His-tag placed adjacent to the SpyTag sequence ensured the latter was retained in the final, purified pigment-protein (Fig. 3b).

The starting point for production of the designed LHCII holoprotein was a pET-28a vector containing a gene encoding the Lhcb1.3 protein from *Arabidopsis thaliana* (UniProtKB entry P04778), that was a kind gift from Prof. Roberta Croce, Vrije Universiteit Amsterdam. Modification of this gene was carried out by Gibson assembly using oligonucleotides sourced from Eurofins or using the Q5® Site-Directed Mutagenesis Kit from NEB. Designed apoproteins were expressed in *E. coli* Rosetta™ 2 (Novagen), purified from inclusion bodies, and the mature pigment-protein assembled *in vitro* using purified chlorophyll *a*, chlorophyll *b* and carotenoid pigments with DDM as the supporting detergent, according to a previously published protocol[35] with exception that ß-mercaptoethanol was replaced by dithiothreitol (DTT). Pigments were purified as described previously[35] with the exception that they were dried from acetone solution using a freeze drier rather than a centrifugal vacuum concentrator. Pigment concentration and composition was determined in 80 % (v/v) acetone using published equations[45].

Each refolded LHCII was first purified by nickel affinity chromatography and then by gel filtration chromatography. Fractions with the lowest A_{470} to A_{674} ratio and invariant emission profiles in response to 440 nm, 475 nm and 500 nm excitation were kept and pooled. Purified proteins were stored at -80°C before use as concentrated solutions in Tris/DDM. An extinction coefficient at the chlorophyll *a* Q_y band equal to 546,000 M^{-1} cm^{-1} was used to estimate LHCII concentration[46].

The four refolded LHCII complexes had absorbance spectra that were similar to one another (Supplementary Fig. S4b) and to spectra previously published by others[35–38]. Their emission spectra were highly similar (Supplementary Fig. S4c), and the line-shapes of these spectra were invariant with excitation wavelength (Supplementary Fig. S4d), a feature diagnostic of a structurally-intact LHCII. Pigment compositions were similar to those typically reported for recombinant LHCII (Supplementary Fig. S4e)[38].

LHCI modification, refolding and purification. LHCI heterodimeric complexes were assembled from modified versions of *A. thaliana* proteins Lhca1 (UniProtKB entry Q01667) and Lhca4 (UniProtKB entry P27521). The mature Lhca1 was modified at its N-terminus either with a Myc protein purification affinity tag (termed L1) or with a Myc-tag followed by the shortened ten amino acid SpyTagΔ (termed Td-L1), and the mature Lhca4 was modified at its N-terminus with a His-tag followed by SpyTagΔ (termed Td-L4) (Fig. 3c and Supplementary Figure S4a). combining L1 or Td-L1 with Td-L4 produced LHCI heterodimers with either one (LHCI-Td) or two (Td-LHCI-Td) SpyTag adaptations.

Expression plasmids were pET-28a containing synthetic genes sourced from Eurofins. Following apoprotein expression in *E. coli*, LHCI heterodimers were assembled by refolding with purified pigments in DDM[26,28,30,39,40]. A 20 % excess (by mass) of either L1 or Td-L1 was mixed with Td-L4 to ensure a minimal level of free Td-L4 monomer after refolding. The apoprotein:total pigment ratio was kept the same as for LHCII refolding. Nickel affinity chromatography was used to separate the His-tagged LHCI dimer from residual Lhca1 monomer (which was not His-tagged). Each LHCI was then further purified by gel filtration chromatography and stored at -80°C before use as a concentrated solution in Tris/DDM. An extinction coefficient for the chlorophyll *a* Q_y band equal to 1,092,000 M^{-1} cm^{-1} was used to evaluate LHCI concentration since its chlorophyll *a* content is approximately twice that of a refolded LHCII monomer[26].

Chimera formation and verification. The standard approach to chimera formation was to mix RCs with a two-fold molar excess of LHCII, or a three-fold molar excess of LHCI, and then separate the chimera from unreacted components by gel filtration chromatography, using absorbance spectroscopy to assess the RC:LHC molar ratio in each column fraction (see sample data in Supplementary Fig. S5c and S6c).

Formation of chimeras was initially verified by sucrose density gradient ultracentrifugation (Fig. 3d,i). Linear sucrose gradients were prepared by freezing and thawing 10 mL of 21 % (w/v) sucrose in 20 mM Tris/0.04% DDM (pH 8.0). Each gradient was loaded with 400 µL of sample with each photoprotein at a concentration of 2.5 µM and then capped with 1 mL of 20 mM Tris/0.04% DDM (pH 8.0). Gradients were ultracentrifuged in a Sorvall TH-641 swing-out rotor at 38,000 rpm for 18 hours at 4 °C.

The protocol for blue-native PAGE was adapted from one published previously[47]. Precast NativePAGE 4-20 % gels purchased from Thermo were run in a Bis-Tris buffer system. Coomassie

blue dye at 0.02 % (w/v) was used in the cathode buffer but not in the loading buffer. The gel cassette was placed in an ice bath and run at 150 V for 1 h followed by 250 V for 2 h.

SDS-PAGE was carried out using precast 4-20 % gradient gels (Bio-Rad). A standard loading of 20 pmol RC was used. Loaded gels were run at 200 V for 45 mins and stained overnight at room temperature with Quick Coomassie Stain (Generon™) after partial protein transfer for western blotting.

Western blotting was carried out following partial protein transfer onto a nitrocellulose membrane (GE Healthcare) on a TE 77 PWR Semi-Dry Transfer Unit (45 mA/gel and 30 min with a NOVA Blot kit). The membrane was then blocked overnight with 5 % milk PBS-Tween (PBS/T) buffer and then incubated with horse radish peroxidase (HPR) conjugated antibodies in the same buffer for 1 h. The membrane was developed using 1x LumniGLO(R) (CST®) after rinsing the membrane three times with PBS/T buffer. Finally, the result was recorded on an ODYSSEY imaging system (LI-COR Biosciences). Re-probing of the membrane was accomplished by stripping and a repeat process of incubation in 5 % milk PBS/T buffer. Stripping of membrane was achieved by incubating twice in mild stripping buffer (200 mM glycine, 0.1 % SDS (w/v), 1 % Tween 20 (v/v), pH 2.2) for 5 mins and twice in TBST buffer (50 mM Tris, 150 mM NaCl, 0.1 % Tween 20 (v/v), pH 7.6), before finally transferring in PBS/T.

Spectroscopy. Absorbance spectra were recorded on a Varian Cary60 spectrophotometer and emission spectra on a Varian Cary Eclipse Fluorimeter in nitrogen-gassed Tris/DDM supplemented with 200 μg/mL glucose oxidase, 7.5 mg/mL glucose, and 35 μg/mL catalase to scavenge oxygen[48].

Photo-oxidation of the RC P870 primary electron donor was measured using an optical fibre attachment for the Cary60 and a four-way cuvette holder (Ocean Optics, Inc.). For excitation, light from a HL-2000 tungsten halogen source (Ocean Optics, Inc.) was passed through an optical fibre and a 25 nm band-pass filter centred at 650 nm (Edmund Optics Ltd). Incident light intensity was approximately 0.3 mW, which yielded $P870^+$ in 5 – 15 % of the RC population. Light-on/off was controlled using the electronic shutter on the light source triggered by a TGP110 pulse generator (Aim-TTi Ltd, United Kingdom). After incubation with a 10-fold excess of ubiquinone-0 (UQ_0) in the dark for 10 mins, samples at a RC concentration of 0.5 μM (0.25 μM with LHCI-Td) were housed in a 3 mm path length, four-sided micro cuvette (110-15-QS, Hellma® Analytics). Each measurement was repeated five times and averaged traces were fitted to a model assuming a simple interconversion between the ground and photo-oxidised state:

$$P870 \underset{k_r}{\overset{k_f}{\leftrightarrow}} P870^{+} \qquad (1)$$

Parameters k_f and k_r from these fits are shown in Supplementary Table S2.

Photochronoamperometry and EQE action spectra. Nanostructured silver electrodes of 2 mm diameter were prepared as described previously[20]. Pigment-proteins at concentrations between 20 µM and 100 µM were drop-casted onto prepared electrodes in the dark at 4 °C for one hour and unbound protein was removed by repeated mechanically-controlled dipping in 20 mM Tris (pH 8) at 4 °C. Coated electrodes were immersed in 20 mM Tris (pH 8)/50 µM KCl/20 µM cyt *c*/1.5 mM ubiquinone-0 (Q_0) in a room temperature electrochemical cell fitted with an Ag/AgCl/3M KCl reference electrode and a platinum counter electrode. Photocurrents were measured at a bias potential of -50 mV vs Ag/AgCl, controlled by a PGSTAT128N potentiostat (Metrohm Autolab). Illumination was supplied by 870 nm or 680 nm LED (Roithner Lasertechnik) with irradiances of 32 or 6.7 mW cm^{-2}, respectively, at the electrode surface (~50 nm FWHM for both). EQE action spectra were recorded using a tungsten-halogen or xenon light source passed through a monochromator, as described previously[20].

Transmission electron microscopy. Negative stain TEM was carried out on an equimolar mixture of 500 nM WT RCs and dLHCII or 500 nM LHCII#RCC heterodimers. A drop of sample was incubated on a glow discharge treated carbon coated grid for 30 s. Filter paper was used to remove excess liquid, the grid was floated on top of a 3 % uranyl acetate (Sigma) droplet, and excess liquid removed again. After one repeat of this procedure the grid was placed for one minute on a third droplet of uranyl acetate and then completely dried in air before imaging with a FEI Tecnai 12 120kV BioTwin Spirit TEM.

Estimation of energy transfer efficiency. Apparent efficiencies of energy transfer were calculated from LHC emission spectra (E_{FL}) using:

$$E_{FL} = 1 - \frac{FL_{chimera}}{FL_{WTRC+LHC}} \qquad (2)$$

where $FL_{chimera}$ was the intensity of LHC emission in a chimera and $FL_{WTRC\ +\ LHC}$ was that in a concentration-matched mixture of the appropriate LHCII or LHCI variant and the WT RC. The same approach was used for estimating the apparent energy transfer efficiency in the mixtures of WT RCs

and LHCII or LHCI, expressing $FL_{WTRC+LHC}$ as a function of the emission from the same concentration of the LHC (FL_{LHC}). For LHCII, where the line shape of the emission spectrum did not vary as it is a single quantum system[49], maximum emission values were used in Eq. 2 as a simple measure of emission intensity. For LHCI, which has multiple distinct emission states[30], values of emission intensity (FL_{int}) were produced by integration across the emission spectrum using Eq. 3, and then applied in Eq. 2.

$$FL_{int} = \int \frac{\lambda}{hc} FL_{LHCI}(\lambda) d\lambda \qquad (3)$$

Apparent efficiencies of energy transfer were also calculated from the rate of P870 photobleaching (k_f) from the kinetic analyses summarised in Supplementary Table S2. To enable this the intensity of the 650 nm excitation light used in these experiments was kept low such that no more than ~15 % of P870 was oxidised within the lifetime of $P870^+$ (~ 1s), ensuring that photooxidation directly represented the quantity of energy received by either direct absorption by the RC or energy transfer from the tethered LHC. The apparent efficiency of energy transfer (E_{P870}) was estimated from the rate of P870 photobleaching using:

$$E_{P870} = \frac{k_f(chimera) - k_f(RC)}{k_f(RC)} \frac{\int P(\lambda)(1 - 10^{Abs_{RC}(\lambda)}) d\lambda}{\int P(\lambda)(1 - 10^{Abs_{LHC}(\lambda)}) d\lambda} \qquad (4)$$

where k_f was the rate of P870 oxidation in a chimera (*chimera*) or the equivalent RC-only control (*RC*) (Supplementary Table S2). Integration of incident photon flux (*P*) and the 1-transmission of RCs or LHCs as a function of wavelength provided the number of photons absorbed by either RCs or LHCIIs per unit area per second (Supplementary Table S2).

For RC1#LHCI#RC1 chimeras there were two acceptors per LHCI, one connected to the Lhca1 subunit and one to the Lhca4 subunit. Efficiencies of energy transfer to the Lhca1-connected RC (E_{a1}) were estimated from:

$$E_{FL,P870} = \frac{E_{a1} + E_{a4} - 2E_{a1}E_{a4}}{1 - E_{a1}E_{a4}} \qquad (5)$$

where $E_{FL,P870}$ was the apparent energy transfer efficiency for the RC#LHCI#RC chimera estimated from either LHC fluorescence or P870 photobleaching and E_{a4} was the corresponding apparent energy transfer efficiency for the LHCI#RC chimera where the single RC is attached to Lhca4. From E_{FL} the value of E_{a1} was 11.5 % (compared to E_{a4} = 19.7 %) and from E_{P870} the value of E_{a1} was 13.9 % (compared to E_{a4} = 20.1 %).

Protein structures and chimera modelling. Protein structures used were Protein Data Bank entries 3ZUW for the *Rba. sphaeroides* RC[50], 2BHW for the LHCII from pea[23], 4KX8 for the LHCI from pea[29] and 4MLI for SpyCatcher/Tag[34]. Schematic models of chimeras were produced using Modeller[51].

References

1. Kolber, Z. S. *et al.* Contribution of aerobic photoheterotrophic bacteria to the carbon cycle in the ocean. *Science* **292,** 2492–2495 (2001).
2. Croce, R. & van Amerongen, H. Natural strategies for photosynthetic light harvesting. *Nat. Chem. Biol.* **10,** 492–501 (2014).
3. Saer, R. G. & Blankenship, R. E. Light harvesting in phototrophic bacteria: structure and function. *Biochem. J.* **474,** 2107–2131 (2017).
4. Scholes, G. D., Fleming, G. R., Olaya-Castro, A. & van Grondelle, R. Lessons from nature about solar light harvesting. *Nat. Chem.* **3,** 763–774 (2011).
5. Zinth, W. & Wachtveitl, J. The first picoseconds in bacterial photosynthesis - Ultrafast electron transfer for the efficient conversion of light energy. *ChemPhysChem* **6,** 871–880 (2005).
6. Jones, M. R. The petite purple photosynthetic powerpack. *Biochem. Soc. Trans.* **37,** 400–407 (2009).
7. Blankenship, R. E. *et al.* Comparing photosynthetic and photovoltaic efficiencies and recognizing the potential for improvement. *Science* **332,** 805–809 (2011).
8. Ort, D. R. *et al.* Redesigning photosynthesis to sustainably meet global food and bioenergy demand. *Proc. Natl. Acad. Sci.* **112,** 8529–8536 (2015).
9. Wang, F., Liu, X. & Willner, I. Integration of photoswitchable proteins, photosynthetic reaction centers and semiconductor/biomolecule hybrids with electrode supports for optobioelectronic applications. *Adv. Mater.* **25,** 349–377 (2013).
10. Nguyen, K. & Bruce, B. D. Growing green electricity: Progress and strategies for use of Photosystem I for sustainable photovoltaic energy conversion. *Biochim. Biophys. Acta - Bioenerg.* **1837,** 1553–1566 (2014).
11. Yehezkeli, O., Tel-Vered, R., Michaeli, D., Willner, I. & Nechushtai, R. Photosynthetic reaction center-functionalized electrodes for photo-bioelectrochemical cells. *Photosynth. Res.* **120,** 71–85 (2014).
12. Ravi, S. K. & Tan, S. C. Progress and perspectives in exploiting photosynthetic biomolecules for solar energy harnessing. *Energy Environ. Sci.* **8,** 2551–2573 (2015).
13. Friebe, V. M. & Frese, R. N. Photosynthetic reaction center-based biophotovoltaics. *Curr. Opin. Electrochem.* **5,** 126–134 (2017).
14. Milano, F., Punzi, A., Ragni, R., Trotta, M. & Farinola, G. M. Photonics and optoelectronics with bacteria: making materials from photosynthetic microorganisms. *Adv. Funct. Mater.* **1805521,** 1–17 (2018)
15. Ravi, S. K. *et al.* Photosynthetic bioelectronic sensors for touch Perception, UV-detection, and nanopower generation: toward self-powered e-skins. *Adv. Mater.* **30**, 1802290 (2018).
16. Sokol, K. P. *et al.* Bias-free photoelectrochemical water splitting with Photosystem II on a dye-sensitized photoanode wired to hydrogenase. *Nat. Energy* **3,** 944–951 (2018).
17. Tan, S. C., Crouch, L. I., Jones, M. R. & Welland, M. Generation of alternating current in response to discontinuous illumination by photoelectrochemical cells based on

photosynthetic proteins. *Angew. Chemie - Int. Ed.* **51,** 6667–6671 (2012).
18. Mirvakili, S. M. *et al.* Photoactive electrodes incorporating electrosprayed bacterial reaction centers. *Adv. Funct. Mater.* **24,** 4789–4794 (2014).
19. Yaghoubi, H. *et al.* Large photocurrent response and external quantum efficiency in biophotoelectrochemical cells incorporating reaction center plus light harvesting complexes. *Biomacromolecules* **16,** 1112–1118 (2015).
20. Friebe, V. M. *et al.* Plasmon-enhanced photocurrent of photosynthetic pigment proteins on nanoporous silver. *Adv. Funct. Mater.* **26,** 285–292 (2016).
21. Ravi, S. K. *et al.* A mechanoresponsive phase-changing electrolyte enables fabrication of high-output solid-state photobioelectrochemical devices from pigment-protein multilayers. *Adv. Mater.* **30,** 1–8 (2018).
22. Liu, Z. *et al.* Crystal structure of spinach major light-harvesting complex at 2.72 Å resolution. *Nature* **428,** 287–292 (2004).
23. Standfuss, J., van Scheltinga, A. C. T., Lamborghini, M. & Kühlbrandt, W. Mechanisms of photoprotection and nonphotochemical quenching in pea light-harvesting complex at 2.5 Å resolution. *EMBO J.* **24,** 919–928 (2005).
24. Su, X., Wei, X., Zhu, D., Chang, W. & Liu, Z. Structure and assembly mechanism of plant C2S2M2-type PSII-LHCII supercomplex. *Science* **820,** 815–820 (2017).
25. van Bezouwen, L. S. *et al.* Subunit and chlorophyll organization of the plant Photosystem II supercomplex. *Nat. Plants* **3,** 1–11 (2017).
26. Croce, R., Morosinotto, T., Castelletti, S., Breton, J. & Bassi, R. The Lhca antenna complexes of higher plants Photosystem I. *Biochim. Biophys. Acta - Bioenerg.* **1556,** 29–40 (2002).
27. Ben-Shem, A., Frolow, F. & Nelson, N. Crystal structure of plant Photosystem I. *Nature* **426,** 630–635 (2003).
28. Wientjes, E. & Croce, R. The light-harvesting complexes of higher-plant Photosystem I: Lhca1/4 and Lhca2/3 form two red-emitting heterodimers. *Biochem. J.* **433,** 477–485 (2011).
29. Qin, X., Suga, M., Kuang, T. & Shen, J.-R. Structural basis for energy transfer pathways in the plant PSI-LHCI supercomplex. *Science* **348,** 989–995 (2015).
30. Krüger, T. P. J., Wientjes, E., Croce, R. & van Grondelle, R. Conformational switching explains the intrinsic multifunctionality of plant light-harvesting complexes. *Proc. Natl. Acad. Sci.* **108,** 13516–13521 (2011).
31. Friebe, V. M. *et al.* On the mechanism of ubiquinone mediated photocurrent generation by a reaction center based photocathode. *Biochim. Biophys. Acta - Bioenerg.* **1857,** 1925–1934 (2016).
32. Friebe, V. M., Millo, D., Swainsbury, D., Jones, M. R. & Frese, R. N. Cytochrome c provides an electron-funneling antenna for efficient photocurrent generation in a reaction center biophotocathode. *ACS Appl. Mater. Interfaces* **9,** 23379–23388 (2017).
33. Zakeri, B. *et al.* Peptide tag forming a rapid covalent bond to a protein, through engineering a bacterial adhesin. *Proc. Natl. Acad. Sci. U. S. A.* **109,** 690–697 (2012).
34. Li, L., Fierer, J. O., Rapoport, T. A. & Howarth, M. Structural analysis and optimization of the covalent association between SpyCatcher and a peptide tag. *J. Mol. Biol.* **426,** 309–317 (2014).
35. Natali, A., Roy, L. M. & Croce, R. In vitro reconstitution of light-harvesting complexes of plants and green algae. *J. Vis. Exp.* **92,** 1–13 (2014).
36. Hobe, S., Prytulla, S., Kuhlbrandt, W. & Paulsen, H. Trimerization and crystallization of reconstituted light-harvesting chlorophyll a/b complex. *EMBO J.* **13,** 3423–3429 (1994).
37. Caffarri, S., Croce, R., Cattivelli, L. & Bassi, R. A look within LHCII: Differential analysis of the

Lhcb1-3 complexes building the major trimeric antenna complex of higher-plant photosynthesis. *Biochemistry* **43,** 9467–9476 (2004).

38. Croce, R., Weiss, S. & Bassi, R. Carotenoid-binding sites of the major light-harvesting complex II of higher plants. *J. Biol. Chem.* **274,** 29613–29623 (1999).
39. Schmid, V. H., Cammarata, K. V, Bruns, B. U. & Schmidt, G. W. In vitro reconstitution of the Photosystem I light-harvesting complex LHCI-730: heterodimerization is required for antenna pigment organization. *Proc. Natl. Acad. Sci. U. S. A.* **94,** 7667–7672 (1997).
40. Passarini, F., Wientjes, E., van Amerongen, H. & Croce, R. Photosystem I light-harvesting complex Lhca4 adopts multiple conformations: Red forms and excited-state quenching are mutually exclusive. *Biochim. Biophys. Acta - Bioenerg.* **1797,** 501–508 (2010).
41. Veggiani, G. *et al.* Programmable polyproteams built using twin peptide superglues. *Proc. Natl. Acad. Sci.* **113,** 1202–1207 (2016).
42. Buldun, C. M., Jean, J. X., Bedford, M. R. & Howarth, M. SnoopLigase catalyzes peptide-peptide locking and enables solid-phase conjugate isolation. *J. Am. Chem. Soc.* **140,** 3008–3018 (2018).
43. Swainsbury, D. J. K., Friebe, V. M., Frese, R. N. & Jones, M. R. Evaluation of a biohybrid photoelectrochemical cell employing the purple bacterial reaction centre as a biosensor for herbicides. *Biosens. Bioelectron.* **58,** 172–178 (2014).
44. Jones, M. R. *et al.* Mutants of *Rhodobacter sphaeroides* lacking one or more pigment-protein complexes and complementation with reaction-centre, LH1, and LH2 genes. *Mol. Microbiol.* **6,** 1173–1184 (1992).
45. Lichtenthaler, H. & Wellburn, A. Determinations of total carotenoids and chlorophylls *b* of leaf extracts in different solvents. *Biochem. Soc. Trans.* **11,** 591–592 (1983).
46. Werwie, M., Fehr, N., Xu, X., Basché, T. & Paulsen, H. Comparison of quantum dot-binding protein tags: affinity determination by ultracentrifugation and FRET. *Biochim. Biophys. Acta - Gen. Subj.* **1840,** 1651–1656 (2014).
47. Ma, J. & Xia, D. The use of blue native PAGE in the evaluation of membrane protein aggregation states for crystallization. *J. Appl. Crystallogr.* **41,** 1150–1160 (2008).
48. Krüger, T. P. J. *et al.* Disentangling the low-energy states of the major light-harvesting complex of plants and their role in photoprotection. *Biochim. Biophys. Acta - Bioenerg.* **1837,** 1027–1038 (2014).
49. Krüger, T. P. J., Novoderezhkin, V. I., Ilioaia, C. & Van Grondelle, R. Fluorescence spectral dynamics of single LHCII trimers. *Biophys. J.* **98,** 3093–3101 (2010).
50. Gibasiewicz, K. *et al.* Mechanism of recombination of the $P^+H_A^-$radical pair in mutant *Rhodobacter sphaeroides* reaction centers with modified free energy gaps between $P^+B_A^-$ and $P^+H_A^-$. *J. Phys. Chem. B* **115,** 13037–13050 (2011).
51. Webb, B. & Sali, A. Comparative protein structure modeling using MODELLER. *Curr. Protoc. Bioinforma.* **15,** 5.6.1-5.6.30 (2016).

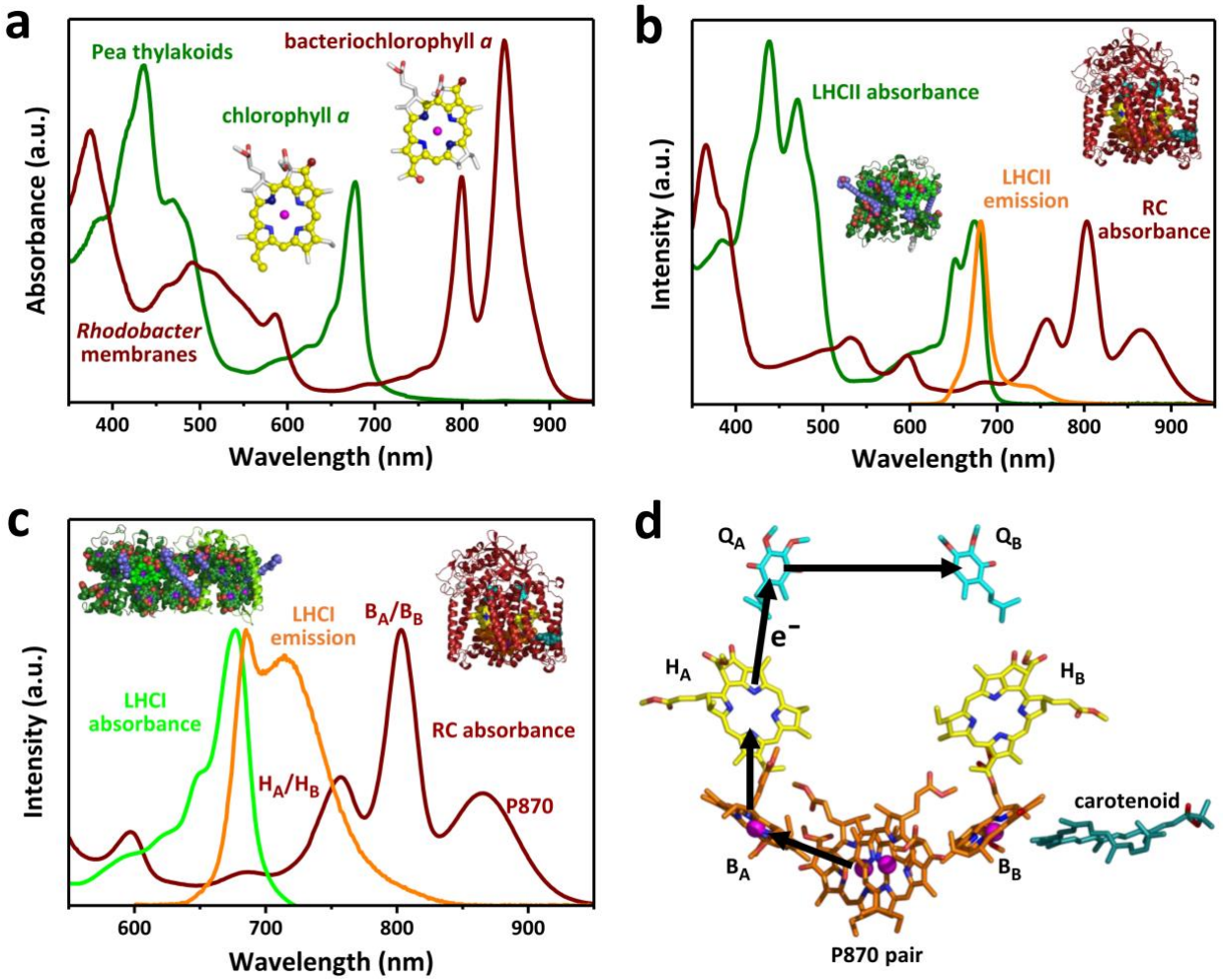

Fig. 1 | Component absorbance, emission and mechanism. a, Thylakoid membranes from oxygenic phototrophs such as pea and chromatophore membranes from anoxygenic phototrophs such as *Rba. sphaeroides* have complementary absorbance spectra due to differences in the electronic structures of the macrocycle π electron systems of chlorophyll and bacteriochlorophyll (see also Supplementary Fig. S1). **b**, The major plant light harvesting complex LHCII harvests solar energy in regions where absorbance by *Rba. sphaeroides* RCs is weak, and its emission spectrum overlaps the absorbance spectrum of the RC between 600 nm and 800 nm. **c**, The red-enhanced emission spectrum of heterodimeric plant LHCI has a stronger overlap with the absorbance spectrum of the *Rba. sphaeroides* RC, particularly the coincident absorbance bands of the bacteriopheophytins (H_A/H_B). **d**, Structure of the RC cofactors and the route of four-step charge separation which oxidises P870 and reduces Q_B. The bacteriochlorophylls (orange carbons) and bacteriopheophytins (yellow carbons) give rise to the absorbance bands labelled in **c**. Further descriptions of pigment-protein structures and their sources are given in Supplementary Fig. S1.

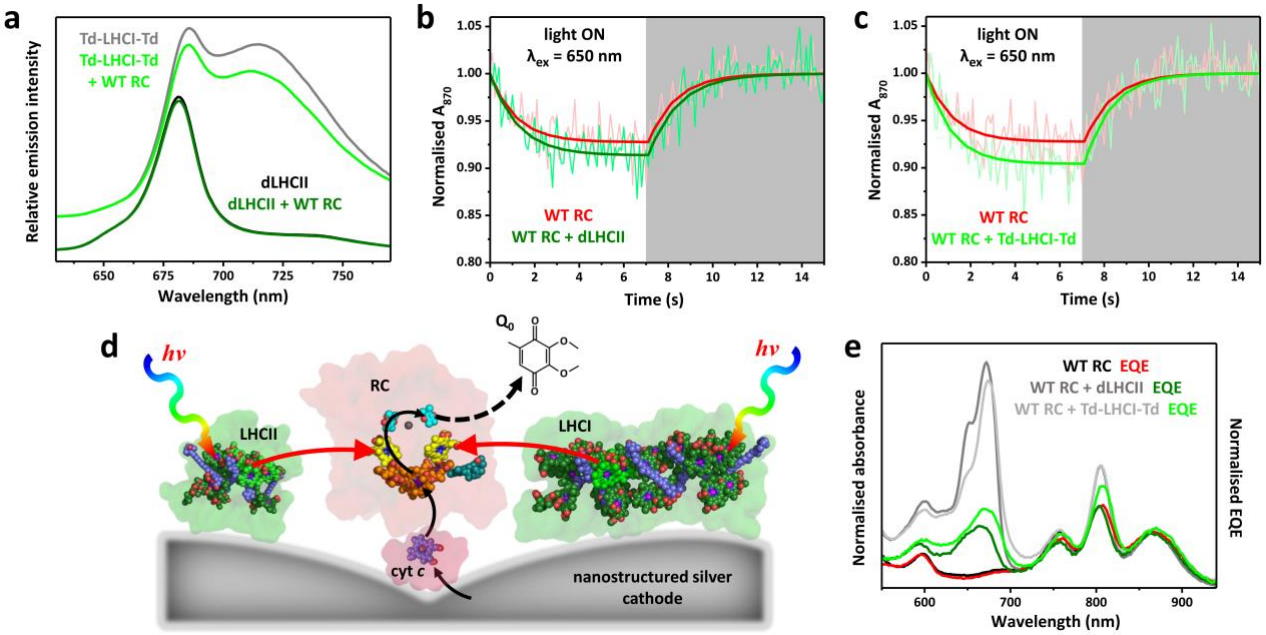

Fig. 2 | Energy confinement in unadapted proteins in solution. a, LHCII emission in the absence and presence of WT RCs (excitation at 475 nm) and LHCI emission in the absence and presence of WT RCs (excitation at 500 nm). The latter spectra are offset for clarity. **b**, Data and fits for photobleaching and dark recovery of P870 absorbance for the WT RC in the absence and presence of LHCII (using variant dLHCII). **c**, Photobleaching and dark recovery of P870 absorbance in WT RCs in the absence and presence of LHCI (using variant Td-LHCI-Td). **d**, Schematic of photocurrent generation on a nanostructured silver electrode; black arrows show the route of electron transfer, cyan arrows show energy flow. **e**, Solution absorbance and EQE spectra for WT RCs compared with those for 1:1 mixtures of WT RCs and dLHCII or Td-LHCI-Td. The absorbance spectra were normalised at 804 nm, whilst each EQE spectrum was normalised to the corresponding absorbance spectrum at the maximum of the P870 band. For **b** and **c** kinetic constants from the fits, carried out as described in Materials and Methods, are summarised in Supplementary Table S2.

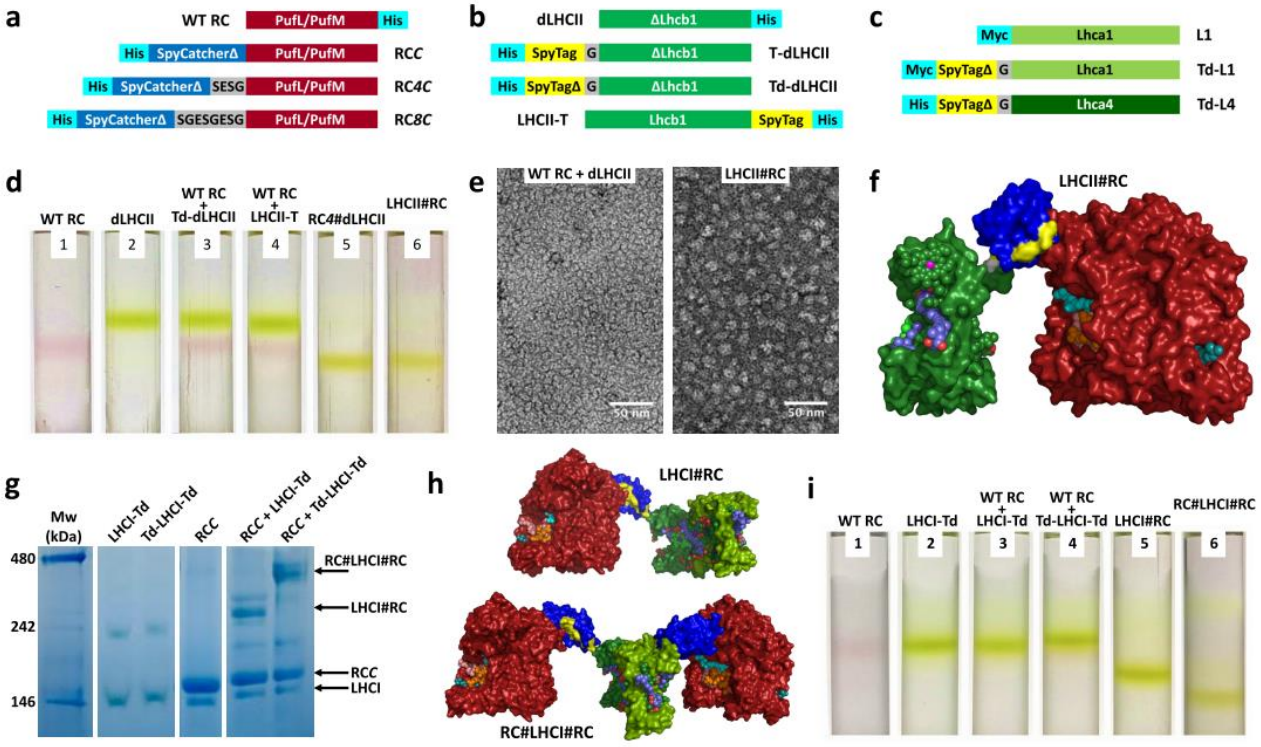

Fig. 3 | Engineering of RC-LHC chimeras. a, Construct designs for adaptation of the RC. For purification the WT RC was modified with a His-tag on PufM. **b**, Construct designs for adaptation of LHCII. The control LHCII was truncated at its N-terminus (dLHCII – see text) and was His-tagged at its C-terminus. **c**, Construct designs for adaptation of LHCI which is a Lhca1/Lhca4 heterodimer. For **b** and **c** protein sequences are given in Supplementary Fig. S4a. **d**, Sucrose density gradient fractionation of RCs (red bands) and LHCII complexes (green bands). RC-LHCII chimeras migrate to a lower position in gradients than either RC or LHCII monomers, with no dissociation into components. **e**, TEM images of (left) an equimolar mixture of the WT RC and dLHCII and (right) the purified LHCII#RC chimera. **f**, Molecular model of the LHCII#RC chimera. The RC (maroon) N-terminally adapted with SpyCatcherΔ (blue) is covalently linked to LHCII (green) C-terminally adapted with SpyTag (yellow). Cofactor colours are as described in Supplementary Fig. S1. **g**, Blue native PAGE showing the formation of high molecular weight products by mixing LHCI-Td or Td-LHCI-Td with RC*C* (see Supplementary Fig. S6a for the full gel with other combinations of LHCI and RC variants). The multiple bands seen for the high molecular weight products are likely to be due to conformational heterogeneity. **h**, Molecular models of the LHCI#RC and RC#LHCI#RC chimeras. Colours as for panel **c** and Supplementary Fig. S1. **i**, Sucrose density gradient fractionation of RCs (red bands) and LHCI complexes (green bands). LHCI#RC chimeras and larger RC#LHCI#RC chimeras migrate to lower positions than either RCs or LHCI.

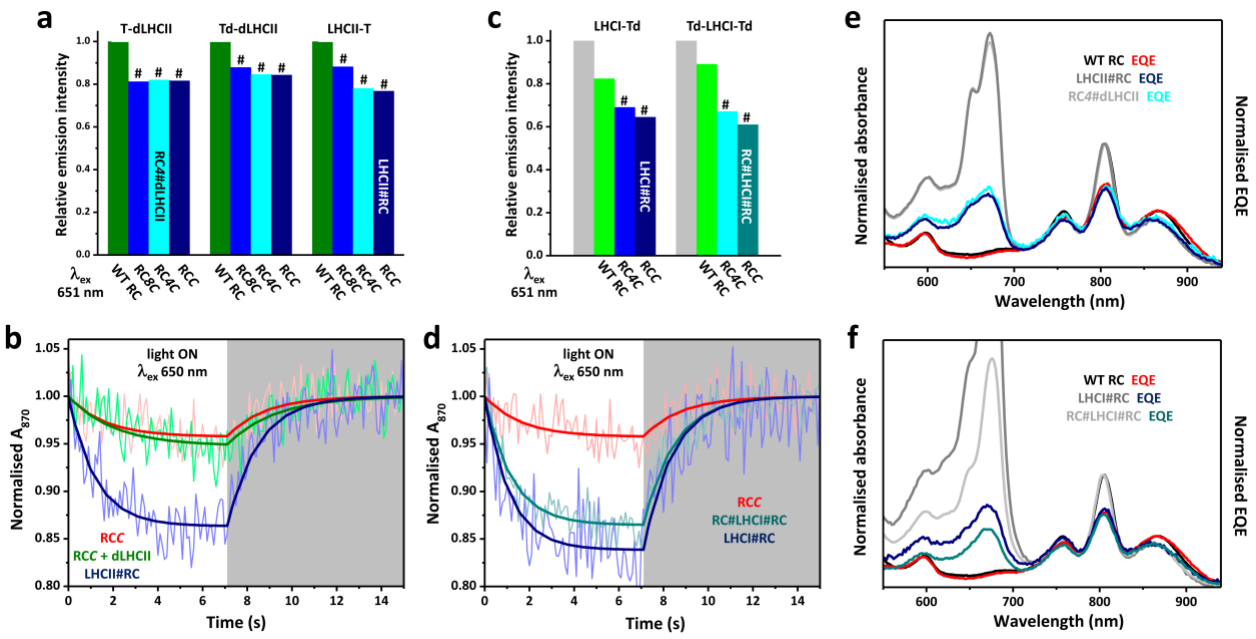

Fig. 4 | Energy transfer in chimeras in solution. **a**, LHCII emission at 681 nm from mixtures with a 2:1 RC:LHCII composition. Emission from LHCII in chimeras (shades of blue) is expressed relative to that from the same LHCII mixed with WT RCs (green). Symbol # denotes mixtures where LHCII has self-assembled into chimeras. Mixtures containing the two chimeras analysed in depth are labelled. **b**, Data and fits for photobleaching and dark recovery of P870 absorbance in RC*C*, a 1:1 RC*C*:dLHCII mixture and the LHCII#RC chimera. **c**, LHCI emission at 714 nm from mixtures with a 3:1 RC:LHCI composition. Emission from RC-LHCI chimeras (left) or $(RC)_2$-LHCI chimeras (right), and that from a mixture of the same LHCI complex and WT RCs (green) is expressed relative to that from the LHCI complex alone (grey). Symbol # denotes mixtures where LHCI has self-assembled into a chimera. Mixtures containing the two chimeras analysed in depth are labelled. **d**, Data and fits for photobleaching and dark recovery of P870 absorbance in RC*C* and two RC-LHCI chimeras. **e**, Solution absorbance and EQE spectra for WT RCs compared with those for LHCII#RC and RC*4*#dLHCII chimeras. **f**, Solution absorbance and EQE spectra for WT RCs compared with those for LHCI#RC or RC#LHCI#RC chimeras. For **e** and **f** the absorbance spectra were normalised at 804 nm, whilst each EQE spectrum was normalised to the corresponding absorbance spectrum at the maximum of the P870 band. For **c** and **d** kinetic constants from the fits, carried out as described in Materials and Methods, are summarised in Supplementary Table S2.

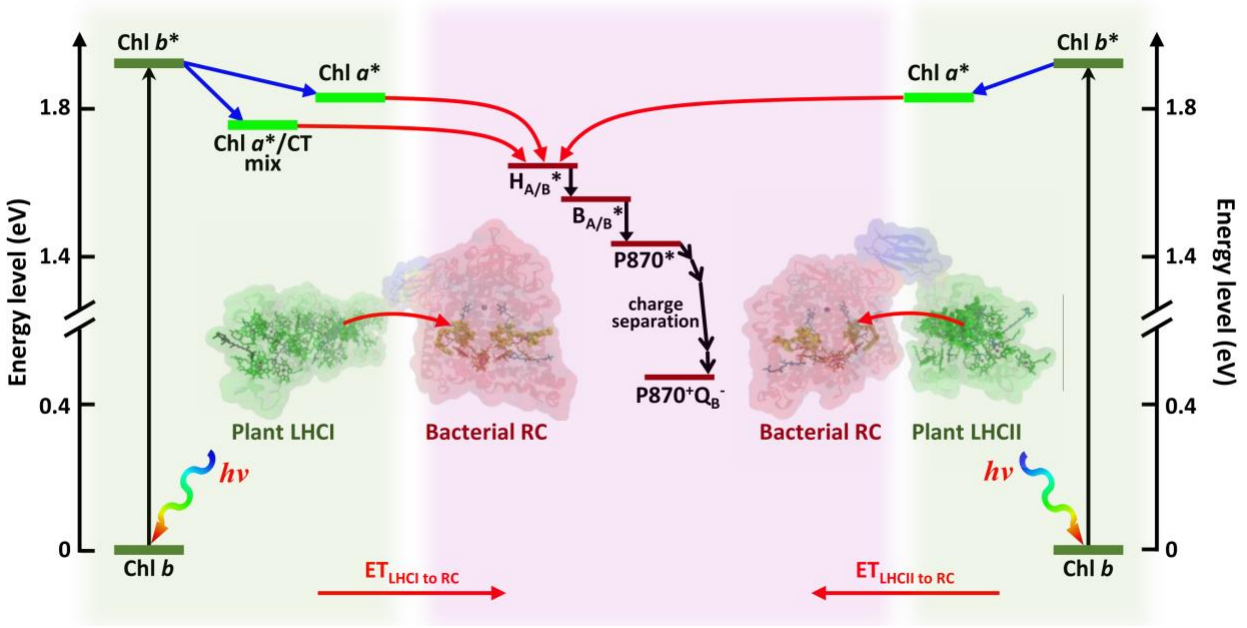

Fig. 5 | Solar energy conversion in chimeras. Energy flow within LHCII or LHCI is from higher energy chlorophyll *b* to lower energy chlorophyll *a*. LHCI also exhibits a red-shifted emissive state with mixed excitonic/charge transfer (CT) character. Excited state energy entering the RC via the bacteriopheophytins ($H_{A/B}$) migrates to the P870 bacteriochlorophylls via the monomeric bacteriochlorophylls ($B_{A/B}$), initiating charge separation to form $P870^+Q_B^-$. Energy harvested by the carotenoid pigments of LHCII or LHCI (not shown) is transferred to the RC via their chlorophylls.

Table 1. Apparent energy transfer efficiencies and associated parameters.

System	E_{P870}	E_{FL}	Relative J[a]	Relative quantum yield[b]
dLHCII				1.00
WT RC + dLHCII	0.8 ± 0.1[c]	2.8 ± 1.1	1.00	
Td-dLHCII				1.02
WT RC + Td-dLHCII	1.9 ± 0.3[c]	0.1 ± 1.4	0.99	
RC*4*#dLHCII	21.7 ± 5.1	17.8 ± 0.2		
LHCII-T				1.04
LHCII-T + WT RC	1.2 ± 0.2[c]	-1.6 ± 1.0	1.00	
LHCII#RC	23.1 ± 4.8	23.8 ± 0.8		
LHCI-Td				0.30
LHCI-Td + WT RC	1.3 ± 0.3[c]	13.4 ± 2.0	1.80	
LHCI#RC	20.1 ± 4.4	19.7 ± 1.1		
Td-LHCI-Td				0.28
$(WT\ RC)_2$ + Td-LHCI-Td	3.8 ± 0.6[c,d]	11.9 ± 4.5[d]	1.83	
RC#LHCI#RC	29.2 ± 5.9[e]	27.3 ± 3.6[e]		

[a] Spectral overlap of LHC emission with RC molar absorbance, normalised to that of dLHCII and RC (SD < 0.01).

[b] Quantum yield relative to that of dLHCII, obtained by comparing integration of LHC emission (SD in the range 0.01 ~ 0.02).

[c] These low apparent energy transfer efficiencies may have arisen from some reabsorption of LHC fluorescence by RCs. In accord with this the maximum percentage of LHC emission that could be reabsorbed by unconjugated RCs in the P870 bleaching measurements was estimated to be ~1-2 % for LHCII and ~1-3 % for LHCI, based on their absorbance.

[d] The variance in these two estimates is attributed to E_{FL} largely reflecting a decrease in LHCI quantum yield on adding WT RCs rather than being due to energy transfer (see text).

[e] RCs conjugated to each of Lhca1 and Lhca4 in the LHCI heterodimer.